Article

Pb(II) binding to humic substances: an equilibrium and spectroscopic study

Siliva Orsetti, José Luis Marco-Brown, Estela María Andrade, and Fernando Victor Molina

Just Accepted

Pb(II) binding to humic substances: an equilibrium and spectroscopic study

Silvia Orsetti†, Jose L. Marco-Brown, Estela M. Andrade and Fernando V. Molina*

AUTHOR ADDRESS: Instituto de Química Física de Materiales, Ambiente y Energía (INQUIMAE), y Departamento de Química Inorgánica, Analítica y Química Física, Facultad de Ciencias Exactas y Naturales, Universidad de Buenos Aires, Buenos Aires, Argentina

AUTHOR EMAIL ADDRESS: fmolina@qi.fcen.uba.ar

BRIEF: Pb(II) is proposed to bind to humic substances in two ways: a relatively strong multiligand complex leading to humic aggregation, and a weaker 1:1 complex.

CORRESPONDING AUTHOR FOOTNOTE: INQUIMAE, Facultad de Ciencias Exactas y Naturales. Ciudad Universitaria, pabellon II, C1428EHA Buenos Aires, Argentina. Tel.: +54-11-4576-3378/80 ext 230. FAX: +54-11-4576-3341. E-mail: fmolina@qi.fcen.uba.ar

†Present address: Institut für Geowissenschaften, Zentrum für angewandte Geowissenschaften, Eberhard-Karls Universität Tübingen, Germany

16   ABSTRACT

17   The binding of Pb(II) to humic acids is studied through an approach combining equilibrium and

18   spectroscopic measurements. The methods employed are potentiometric and fluorometric titrations,

19   fluorescence excitation-emission matrices (EEM) and IR spectroscopy. Potentiometric titration curves

20   are analyzed using the NICA equations and an electrostatic model treating the humic particles as an

21   elastic polyelectrolyte network. EEMs are analyzed using parallel factor analysis, decomposing the

22   signal in its independent components and finding their dependence on Pb(II) activity. Potentiometric

23   results are consistent with bimodal affinity distributions for Pb(II) binding, whereas fluorometric

24   titrations are explained by monomodal distributions. EEM analysis is consistent with three independent

25   components in the humic fluorescence response, which are assigned to moieties with different degree of

26   aromaticity. All three components show a similar quenching behavior upon Pb(II) binding, saturating at

27   relatively low Pb(II) concentrations. This is attributed to metal ion induced aggregation of humic

28   molecules, resulting in the interaction between the aromatic groups responsible for fluorescence; this is

29   also consistent with IR spectroscopy results. The observed behavior is interpreted considering that initial

30   metal binding (observed as strongly binding sites), correspond to bi- or multidentate complexation to

31   carboxylate groups, including binding between groups of different humic molecules, promoting

32   aggregation; further metal ions (observed as weakly binding sites) bind to single ligand groups.

33   KEYWORDS Potentiometric titration; fluorescence spectroscopy; IR spectroscopy; metal-humic

34   binding; affinity spectra.

35

Introduction

36

37   Humic substances (HS) are important components of natural organic matter (NOM) in groundwater

38   and soils[1,2] HS interact with other chemical species in the natural environment, in particular binding

39   heavy metal cations.[3–5] Among different experimental studies, equilibrium binding data, usually titration

40   curves, have been reported and modeled.[3,6–8] Recently, the electrostatic behavior of HS was treated

41   through the elastic polyelectrolyte network model (EPN)[9] which allows for expansion and shrinking as

42   the HS charge changes; it can be combined with the NICA[10] intrinsic isotherm, resulting in the NICA-

43   EPN model which has been applied to proton binding to HS.[9] Fluorescence spectroscopy is an useful

44   tool in the study of metal binding to HS.[4,11] In the last years, excitation-emission matrix (EEM)

45   fluorescence spectroscopy with parallel factor analysis (PARAFAC) was successfully applied for the

46   identification and characterization of NOM.[12–16] For simple mixtures, PARAFAC components are

47   identified with individual fluorophores present; for HS, the identified components represent

48   fluorescence phenomena, which may be individual fluorophores or approximations to the effects of local

49   processes such as intramolecular charge transfer.

50   Even after many research efforts, the exact nature of HS and the way in which they interact with metal

51   cations remains unclear. With the aim of gaining insight in this problem, the binding of Pb(II) to humic

52   acids (HA) is studied here by a combined analysis of titration and spectroscopic experiments.

53   Equilibrium curves are obtained through potentiometric titrations and analyzed with the NICA-EPN

54   model for metal binding to obtain intrinsic binding parameters; also, fluorometric titrations are

55   performed to compare the binding affinities. EEM measurements[17] with PARAFAC analysis[13,18] are

56   conducted to study the behavior of the different fluorophores with Pb(II) additions. Finally, IR-ATR

57   spectra are recorded to study the Pb-HA interactions.

58

Modeling of proton and metal binding data: the NICA-EPN model

59

60   Titration data was analyzed using the NICA isotherm for the intrinsic affinity[7] and the Elastic

61   Polyelectrolyte Network (EPN) submodel[9] for the electrostatic contribution. In the NICA-EPN model,

62   the amount bound of species i per unity of mass in the presence of species j is given by

63    $$Q_i = g_f \sum_{k=1}^{M} \frac{n_{i,k}}{n_{1,k}} Q_{\max,k} \vartheta_{i,k}(a_1^{\text{int}},...,a_j^{\text{int}},...,a_n^{\text{int}}) + (1-g_f) \sum_{k=1}^{M} \frac{n_{i,k}}{n_{1,k}} Q_{\max,k} \vartheta_{i,k}(a_1,...,a_j,...,a_n) + Q_{i,el} \qquad (1)$$

64   where $\vartheta_{i,k}(a_i)$ is the fraction of type k sites occupied by species i, given in the NICA isotherm by

65    $$\vartheta_{i,k}(a_1,...a_j,...,a_n) = \frac{\left(\bar{K}_{i,k}a_i\right)^{n_{i,k}}}{\sum_{j=1}^{n}\left(\bar{K}_{j,k}a_j\right)^{n_{j,k}}} \times \frac{\left[\sum_{j=1}^{N}\left(\bar{K}_{j,k}a_j\right)^{n_{j,k}}\right]^{p_k}}{1+\left[\sum_{j=1}^{N}\left(\bar{K}_{j,k}a_j\right)^{n_{j,k}}\right]^{p_k}} \qquad (2)$$

66   In eqs 1 and 2, N is the number of species binding to the HA, M the number of sites, $Q_{\max}$ the total

67   number of sites per unity of mass, $Q_{\max,k}$ the same for type k sites (assuming 1:1 binding), q_k the fraction

68   of type k sites ($Q_{\max,k} = q_k Q_{\max}$), $n_{i,k}$ the nonideality parameter for species i on type k sites, ($n_{1,k}$ being for

69   H^+), p_k is the heterogeneity parameter of type k sites and $\bar{K}_{i,k}$ is the average binding constant of species i

70   on type k sites. Two site types are considered: low affinity ($k = 1$, attributed to carboxylic groups) and

71   high affinity ($k = 2$, usually attributed to phenolic groups),[7,19] so $M = 2$, and for binding of a metal cation

72   in the presence of protons $N = 2$.

73   As it is widely accepted, HS are actually composed of relatively small molecules and molecular

74   fragments (as opposed to a macromolecular/polymeric view) which are entangled and/or bound by

75   diverse forces, like hydrogen bonding, metal ion bridging, van der Waals interactions, etc. forming

76   particles of supramolecular nature which can shrink and swell.[20,21] In the EPN model,[9] these HS

77   particles are treated, from a purely mechano-statistical point of view, as an elastic network which can

78   exchange ions and solvent with the surrounding solution; further, the particles are considered as divided

79   in two fractions: an inner fraction g_f, which behaves as a gel in Donnan equilibrium with the bulk

80   solution, and an external fraction $1 - g_f$. The humic binding sites outside the gel are in equilibrium with

81   the bulk solution, whereas those inside the gel are in equilibrium at the internal ionic activity, a_j^{int},

82   which is given by

83    $$a_j^{\text{int}} = a_j \exp(-F\psi_D / RT) \qquad (3)$$

84   where ψ_D is the Donnan potential, a_j is the activity in the bulk and F, R and T have their usual meaning.

85   For a 1:1 electrolyte, ψ_D results to be, from the electroneutrality condition,[9]

86
$$\psi_D = \frac{RT}{F} \text{arcsinh}\left(\frac{g_f Q \delta \varphi_2}{2I(1-\varphi_2)} \right) \tag{4}$$

87   where Q is the net charge of the humic particle, δ the density of the dry humic substance (following

88   Dinar[22] $\delta = 1.5$ g cm^{-3}), I the ionic strength, and φ_2 is the volume fraction of the HS in the gel, obtained

89   from the swelling equilibrium condition:[9]

90
$$\frac{1}{v_1}\left[\chi\varphi_2^2 + \varphi_2 + \ln(1-\varphi_2) \right] + \frac{1}{v_2}\left(\varphi_2^{1/3} - \frac{2\varphi_2}{f_P} \right) + 2I\left[1 - \sqrt{1 + \left(\frac{g_f Q \delta \varphi_2}{2I(1-\varphi_2)} \right)^2} \right] = 0 \tag{5}$$

91   where v_1 is the water molar volume, v_2 is the average molar volume of a humic equivalent chain, χ is a

92   Van Laar heat of mixing parameter and f_P is the Flory functionality,[23] which was set equal to 3. $Q_{i,el}$ is

93   the excess amount of species i electrostatically bound in the gel phase:

94
$$Q_{i,el} = \left(c_i^{\text{int}} - c_i \right)\frac{g_f}{\delta\varphi_2} \tag{6}$$

95   where c_i^{int} and c_i are the concentrations of species i in the gel and the bulk solution, respectively. The

96   Davies equation was employed to calculate activity coefficients throughout; it was verified that the ionic

97   strength inside the gel was always within its validity limit ($I < 0.3$ M).

98   As it is well known,[7] eq 2 reduces to a Langmuir-Freundlich isotherm for non competitive (H$^+$) binding:

99
$$\vartheta_{H,k}(a_H) = \frac{\left(\bar{K}_{H,k} a_H \right)^{m_{H,k}}}{1 + \left(\bar{K}_{H,k} a_H \right)^{m_{H,k}}} \tag{7}$$

100   where $m_{H,k} = n_{H,k}\, p_k$.

101   Also, conditional affinity distributions can be obtained using constrained regularization methods.[24] If the

102   proton affinity spectrum $g(\log K_H)$ is known, a conditional metal affinity distribution $f(\log K_M)$ can be

103   estimated solving numerically the equation (assuming uncorrelated proton and metal affinity spectra):[24]

104
$$Q_M = Q_{max} \int_{-\infty}^{\infty} \left[\int_{-\infty}^{\infty} \frac{K_M a_M}{1 + K_H a_H + K_M a_M} g(\log K_H) d\log K_H \right] f(\log K_M) d\log K_M \quad (8)$$

105   where Q_M is the amount of metal bound.

106

107   **Materials and methods**

108   The HAs employed were a purified Fluka humic acid (FHA) and IHSS standard Elliot soil humic acid

109   (EHA); these HS have been characterized in the literature, as presented in Table S1, Supporting

110   Information. Acid-base potentiometric titrations were performed following usual procedures[25] at 1 g L^{-1}

111   HA concentration and different ionic strengths in NaClO$_4$. Pb(II)-humic potentiometric titrations also

112   followed known procedures[10] at pHs of 4.0 and 5.5, and ionic strengths (NaClO$_4$) of 0.1 M and 0.02 M.

113   Fluorometric titrations were performed, at a HA concentration of 20 mg L^{-1}. In order to enable

114   comparisons, binding curves for this concentration were calculated using the fitted model parameters;

115   some potentiometric measurements were also done, but no processed due to the low reliability of ISE

116   measurements at low HA concentrations;[26] however, they reflected the same general tendency.

117   Fluorescence EEMs of 20 mg L^{-1} solutions of HA alone and with increasing amounts of Pb(II) were

118   recorded. UV-Vis spectra were also recorded to check the onset of humic flocculation. IR-ATR

119   spectroscopy measurements of HA-Pb complexes were performed following usual techniques,[27,28] using

120   the electrolyte spectrum as reference to obtain the difference spectra. Experimental details are given in

121   Appendix A, Supporting Information.

122   The data treatment was, briefly, as follows. First from acid-base titration data the humic charge as a

123   function of pH was computed and fitted to the NICA-EPN model, using a constrained Levenberg-

124   Marquardt algorithm,[29] obtaining the corresponding NICA parameters as well as the EPN ones, namely

125   χ, g_f and v_2. Then, curves of Pb(II) binding as a function of Pb(II) activity were obtained from titration

126   data, and also fitted to the NICA-EPN model, taking the proton binding and EPN parameters from the

127   proton experiments.

128   Fluorometric titration data was converted to relative fluorescence quenching, θ_F, defined as:

129     $$\theta_F = \frac{I_F^0 - I_F}{I_F^0 - I_F^\infty}$$ (9)

130   Here, I_F^0 is the fluorescence emission intensity in the absence of Pb(II), I_F^∞ is the intensity observed at

131   maximum quenching and I_F is the intensity at each point. This intensity values can be taken as the

132   intensity at the wavelength of maximum emission or as the integrated emission spectra. Both ways led to

133   the same results. Fluorescence EEMs were converted to Raman units following Stedmon et al.,[18]

134   processed with PARAFAC,[12,13] yielding the number of independent fluorescent phenomena, their

135   absorption and emission spectra, and their relative concentrations (scores) in each sample. The data

136   treatment procedures are detailed in Appendix B, Supporting information.

137

138   **Results and discussion**

139

140   **Potentiometric titrations.** Acid-base titration curve fitting to the NICA-EPN model shows very good

141   agreement (Figure S1, Supporting Information). The intrinsic NICA parameters for proton binding are

142   collected in Table 1, falling in the ranges reported in the literature;[19,30] also included are the total sites

143   (Q_{max}) and the electrostatic parameters g_f, χ and v_2. The proton binding constants found for low affinity

144   sites are close to typical values for isolated carboxylic groups. For the high affinity type sites our results

145   are close to the pK_a for phenol (9.8); it has been reported that in HS most phenolic OH groups are

146   isolated[31,32] which is consistent with these results.

147   The electrostatic parameters g_f and χ are similar to those reported previously;[9] the first one represents

148   the part of the humic particle where the electrostatic potential is on average equal to ψ_D, being about half

149   of the binding sites, whereas a positive value for χ corresponds to a repulsive heat of mixing humic-

150   water, which is expected because HS have a significant fraction of non polar groups. There are

151   significant differences in v_2, quite low for EHA and high for FHA; this parameter is the molar volume of

152   the equivalent chain segments in a network representing the humic particle, thus the results found would

153   indicate that FHA is relatively less entangled whereas EHA would be highly entangled.

154

155 **Table 1.** NICA-EPN model fitting parameters

Proton binding	$\log \overline{K}_{H,1}$	$\log \overline{K}_{H,2}$	Q_{max}/ mol kg^{-1}	q_1	q_2	$m_{H,1}$	$m_{H,2}$	g_f	χ	v_2/ L mol^{-1}
Elliot HA	4.42	9.43	5.0	0.52	0.48	0.51	0.20	0.48	0.47	1.7
Fluka HA	4.44	9.91	5.2	0.56	0.44	0.39	0.23	0.47	0.51	10.2
Pb(II) binding	$\log \overline{K}_{Pb,1}$	$\log \overline{K}_{Pb,2}$	$n_{Pb,1}$	$n_{Pb,2}$	p_1	p_2		N_d [a]	R^2 [b]	RMSE [c]
Elliot HA	0.55	9.8	0.80	0.49	0.70	0.40		228	0.9990	0.058
Fluka HA	0.50	5.8	0.90	0.52	0.49	0.89		209	0.9993	0.039

156   [a] Total data points. [b] $R^2 = 1 - \sum \left(Q_i - Q_{i,calc} \right)^2 / \left[\sum Q_i^2 - \left(\sum Q_i \right)^2 / N_d \right]$. [c] RMSE $= \sqrt{\sum \left(Q_i - Q_{i,calc} \right)^2 / N_d}$.

157

158   Figure 1 shows the results for the HA-Pb titrations with good agreement; the generic NICA-Donnan

159   (ND)[19] predicted curves being also shown for comparison. The pH dependence is similar to that reported

160   by Milne et al.[3] and references therein. The influence of I has been much less studied; here it is observed

161   that the curves at different ionic strengths merge as Pb(II) activity increases; some literature studies

162   show similar behavior: Cu binding to Suwannee River fulvic acid,[33] Am complexation with Gohy-573

163   humic acid,[34] and Cu complexation with Sable silt loam HA[35]. The NICA-EPN model predicts well this

164   dependence, whereas the generic ND curves are nearly parallel. Table 1 collects the Pb intrinsic binding

165   parameters and the fitting quality results for the full data set fitting (proton and metal curves.

166   Figure 2 shows the speciation of bound Pb(II) at pH = 5.5 and I = 0.1 M (other cases are similar),

167   writing eq 1 in the form:

168    $$Q_{Pb} = Q_{Pb,1}^{int} \left(a_H^{int}, a_{Pb}^{int} \right) + Q_{Pb,2}^{int} \left(a_H^{int}, a_{Pb}^{int} \right) + Q_{Pb,1}^{ext} \left(a_H, a_{Pb} \right) + Q_{Pb,2}^{ext} \left(a_H, a_{Pb} \right) + Q_{Pb,el} \qquad (10)$$

169   where $Q_{Pb,k}^{int} = g_f \left(n_{Pb,k} / n_{H,k} \right) Q_{max,k} \vartheta_{Pb,k}(a_{Pb}^{int}, a_{H}^{int})$ and so on. As it is observed, most Pb is bound to high

170   affinity sites in the activity range studied, specially for EHA. From $a_{Pb} \approx 10^{-4}$ up the binding to low

171   affinity sites shows an increase. The electrostatic binding in the gel fraction (eq 6) is negligible in all

172   cases; note also that for FHA this contribution changes sign; this is due to inversion of the gel fraction

173   charge caused by the Pb loading.

174   There are several published studies of Pb binding to HS;[3,36–42] however, direct comparisons are

175   difficult because the different HS and conditions employed. The values of $\bar{K}_{Pb,k}$ found here (with the

176   exception of high affinity sites for EHA) are within the ranges reported by Milne et al.,[3] Gustafsson,[8,40]

177   and Tipping.[6] Puy et al.[37] reported somewhat higher values of $\log \bar{K}_{Pb,1}$ (4.37) and $\log \bar{K}_{Pb,2}$ (7.57). The

178   high affinity constant for EHA found here is higher than the values reported by all these authors; in

179   some studies, Pb(II) binding to soil organic matter was found to be considerably higher than predicted

180   by current models, free Pb being about one order of magnitude lower than predicted (see Gustafsson et

181   al.[40] and references therein). Thus, being EHA a soil HA, whereas FHA is originated from coal, the

182   difference in their $\bar{K}_{Pb,2}$ values is consistent with the findings reported by Gustafsson et al.[40]

183

184   **Fluorometric titrations.** During titration of HA with Pb(II), fluorescent emission is quenched as

185   Pb(II) concentration increases, until a limiting emission is reached, which does not change as Pb(II)

186   concentration is further increased (Figure S2, Supporting Information). In all cases, the lowest emission

187   intensity observed was taken as I_F^{∞} in eq 9 to compute θ_F. This quenching has been observed by a

188   number of researchers and for several cations.[11,43] Along the titrations, the absorbance spectra of the

189   HA-Pb solutions were checked. It was found to remain unchanged until the appearance of flocculation

190   and/or precipitation, were the absorbance started to decrease (Figure S3, Supporting Information); only

191   fluorescence measurements before this point were considered in the analysis, thus in all the results

192   presented here the UV spectra remained constant. Figure 3 compares the results for fluorometric

193   titrations with Pb binding curves calculated with the NICA-EPN model for EHA and FHA. The general

194   features are coincident with previous studies.[3,44,45] It is observed that the results are qualitatively similar

195   but not quantitatively coincident, showing the fluorometric response a tendency to saturation at pPb ~5,

196   which is not observed for the potentiometric curves. This behavior was also observed in preliminary

197   experiments conducted with other cations such as Cu(II) and Mn(II) (not shown). Similar comparisons

198   were done previously by Saar and Weber[43] who measured binding of several cations to fulvic acids,

199   finding good correlation for Cu(II) but only poor agreement for Pb(II), and even poorer for Co(II) and

200   Ni(II). Other studies[11,46] were instead focused on obtaining binding equilibrium constants directly from

201   quenching data.

202

203   **Excitation-Emission matrices.** The EEM plots for Pb(II) binding to HA show typical shapes

204   observed for HS[14,16,47] (Figure S4, Supporting Information). The shape changes as Pb(II) concentration

205   increases; the emission and excitation maxima shift towards lower wavelengths in both cases, but its

206   intensity always decreases with increasing metal concentration. The changes in shape indicate that the

207   EEMs are linearly independent, and consequently are analyzable using PARAFAC.

208   After PARAFAC processing changing the number of fluorophores, N_f, between 1 and 5 it was found,

209   in all cases, that $N_f = 3$ gave an optimal fit of the model, revealed by a low value for residual standard

210   deviation, σ_R, and a high value for core consistency, CC, for that number (Figure S5, Supporting

211   Information). This result is consistent with that reported in literature for IHSS reference humic

212   substances[48] and is also consistent with measurements of fluorescence lifetime of HS, showing three

213   distinct values.[49] Figure 4 shows contour maps of the different fluorophores for EHA and FHA, which

214   are similar to others HA.[13,48,50] The components have been named starting from the emission maximum

215   with the higher wavelength, the spectra showing only a small dependence with pH and ionic strength;

216   Table S2 (Supporting Information) collects the average peak emission and excitation wavelengths for

217   FHA and EHA. The maxima location is related to the fluorophore structure:[18,51] the higher the degree of

218   conjugation, the higher the excitation wavelength; this suggests that the A component is the more

219   aromatic, with aromaticity decreasing in the B and C components. The component C is also observed in

220   fulvic acids.[52] The three have spectral characteristics consistent with the operationally defined humic

221   acids by Chen et al.[53] based on pyrolysis results.[54] The quenching efficiency for these components lies in

222   the same order: the more aromatic is more efficiently quenched. In similar studies with dissolved

223   organic matter and aquatic HS, 13 fluorophores were reported,[55] including aminoacid-like components

224   with emission $\lambda_{em,max} \leq 350$ nm; one of such fluorophores (tyrosine-like) was found[56] to give high

225   deviation from linearity in inner filter effects for A_{254} (the absorbance at 254 nm) > 0.3, all the rest

226   showed low deviations up to $A_{254} \cong 1.0$. In this study, no such fluorophore is found; moreover, the

227   fluorescence titrations are treated as relative values (eq 9) and the HA concentration and the full

228   absorbance spectra are constant in the measurements, thus the correction should be the same for all data,

229   even being nonlinear. Consequently, the PARAFAC resulting spectra were corrected for inner filter

230   effects. In view of the above considerations, the results shown in Figure 5 should be considered as

231   semiquantitative.

232   Figure 5 present typical results for the scores (concentrations) of each fluorophore as a function of

233   total Pb(II) concentration, c^0_{Pb}. Other results are presented in Figures S6 and S7 (Supporting

234   Information). It is seen that component A has the higher scores and shows greater quenching, followed

235   in both aspects by B and then C. Usually, the behavior is similar for all three components; in some

236   cases, the component C shows no observable quenching. No essential differences are found between

237   components; similar results were found by Yamashita and Jaffé.[47]

238

239   **IR-ATR spectra.** In Figure 6 the spectra of EHA in the absence and presence of Pb(II) are shown; as

240   detailed in Appendix B (Supporting Information) the 4000-3000 cm^{-1} was recorded with lower

241   sensitivity due to water band saturation, thus presenting higher noise. The bare EHA spectrum is typical

242   of HS,[2] having relatively broad bands resulting from the multiple chemical environments of the

243   absorbing groups. Here, we will discuss mainly the carboxylic C=O stretching at 1720 cm^{-1} and the

244   carboxylate bands at 1585 (ν_a, asymmetric stretching) and 1380 cm^{-1} (ν_s, symmetric);[57,58] these bands

11

245   are marked in the figure. Also, a sharp band is observed at *ca.* 1105 cm^{-1}, attributed to C-O stretching of

246   polysaccharide-like substances[59] and a weak band at *ca.* 1260 cm^{-1} attributable to phenol groups.[60]

247   Finally, the OH stretching region shows a negative band due to differences in OH absorption between

248   the HA solution and the electrolyte reference.

249   Two spectra with Pb in different concentrations are shown; using NICA-EPN parameters, the metal

250   loadings are estimated as 0.36 and 2.4 mol kg^{-1}, thus these can be considered as representative of low

251   and high loadings, respectively. In the low loading case, the carboxylic band decreases, whereas the

252   carboxylate bands increase and shift to 1564 and 1386 cm^{-1}, respectively, indicating that carboxylate

253   groups are involved in binding; the other bands mentioned do not change, indicating that OH groups are

254   not involved. Under high loading, those changes appear enhanced, except for v_s, where a sharp increase

255   is found and new band arises at 1350 cm^{-1}; the sharp increase has been observed in other cases,[28,59]

256   whereas the new band indicates a different carboxylate binding mode. According to Nakamoto,[58] the

257   difference $\Delta = v_a - v_s$ is indicative of the binding mode, a decrease being attributable to a chelate (metal

258   bound to both O atoms) or a bridging complex (one metal bound to each O atom); here Δ decreases from

259   205 to 178 cm^{-1} at low loading, which is likely due to chelate formation, whereas the new band at high

260   loading shows $\Delta = 208$ cm^{-1}, a small increase which could be indicative of monodentate binding. The C-

261   O bands again do not show changes, whereas in the OH region a small increase is observed, which could

262   be attributable to OH$^-$ ions coordinating the Pb ions; involvement of HA OH groups in binding would

263   result in a decrease due to deprotonation. Thus, we conclude that Pb binding to the HA proceeds via the

264   carboxylate groups in different modes depending on metal loading, without appreciable involvement of

265   OH groups.

266

267   **Affinity spectra.** Figure 7 shows the affinity spectrum for Pb(II) binding to EHA corresponding to the

268   NICA fitting results shown in Table 1, compared with the conditional spectra for fluorometric

269   measurements obtained solving numerically eq 8; similar results are obtained for FHA (Figure S8,

270   Supporting Information); Figure S9 (Supporting Information) shows the NICA affinity distributions for

271   protons. These are bimodal distributions with peaks at log K_{Pb} values ~0.5 for the low affinity sites,

272   being for high affinity 5.8 for FHA and 9.8 for EHA. On the other hand, fluorometric results show

273   monomodal distributions peaking at ~5 for FHA and ~6-7 for EHA, roughly coincident with the higher

274   affinity peak from the potentiometric experiments. This suggests (considering also IR results) that

275   fluorescent quenching is sensing only high affinity sites for Pb(II), whereas potentiometric analysis finds

276   two types. Comparison of potentiometric and fluorometric measurements has been conducted by several

277   researchers,[4,43,61,62] usually finding that metal binding quenches the HS fluorescence; however, it was

278   noted that both techniques do not sense the same complexation phenomena:[4] for Cu binding to fulvic

279   acid, it was observed that the two measurements agreed only at low levels of copper loading,[61] which is

280   consistent with our findings. Also, Saar and Weber found poor agreement between potentiometric and

281   fluorometric measurements for Pb.[43] These binding sites are expected to be, given the IR results,

282   carboxylates; this is also consistent with the fact that carboxylate groups are known to form stable

283   complexes with Pb(II)[63] whereas phenol groups are not expected to bind Pb(II) at the present pH

284   values.[64] There are a number of studies which seek to obtain binding constants between metal cations

285   and humic substances from fluorescence measurements, based on the assumptions of 1:1 binding and

286   that fluorescence was detecting all types of binding sites.[46] However, as already observed by Senesi,[4] the

287   two techniques are not equivalent and, as found here, fluorometry senses only the strongly binding sites.

288   Therefore, the binding constants obtained exclusively through fluorometry should be considered valid

289   only in the context of this technique.

290

291   **Fluorescence quenching.** Quenching of fluorescence can be caused by several mechanisms, mainly

292   dynamic (collisional) and static (complex formation).[51] For single fluorophores, the Stern-Volmer plot, a

293   graphic of I_F^0/I_F as a function of the total quencher concentration, is useful to reveal the type of

294   quenching taking place.[51] For HS, their complex nature introduces difficulties because the observed

295   emission is the result of the combination of several fluorescence phenomena. Here, we treat the

296   PARAFAC components as independent fluorophores to analyze the quenching behavior. In most cases,

297   the Stern-Volmer plots show an upward curvature (Figure S10, Supporting Information); for simple

298   cases, this is indicative of mixed static-dynamic quenching;[51] however dynamic (collisional) quenching

299   is usually important at concentrations several orders of magnitude higher.[65] Furthermore, attempts to

300   deduce quenching parameters by usual methods[51] from these plots lead to unreasonably high values for

301   the dynamic quenching constant. Thus we conclude that static quenching is present in this case, as found

302   before for other metal-HS systems.[4] The effect could be due to different causes;[51] for HS it has been

303   attributed to intersystem crossing;[4] that is, enhanced transference from the singlet excited state to the

304   triplet ground state. Aromatic carboxylic acids show usually this type of quenching.[4,46,61,66] However, in

305   the case of HS this is not necessarily true: some studies[66] show that complexes of model compounds

306   with heavy metal ions (such as Tb(III)) show quenching whereas binding of the same cation to HS does

307   not. Furthermore, a molecular quenching mechanism such as intersystem crossing would require the

308   carboxylic groups to be directly bound to the fluorescent aromatic groups, but this is not necessarily the

309   case: on one hand not all the fluorescent aromatic groups would have a carboxylic substituent, and on

310   the other not every carboxylate would be attached to a fluorophore group.[1,2,4] Thus, we propose as an

311   alternative quenching mechanism the aggregation of humic molecules induced by Pb(II) binding.

312   Quenching by dimerization of aromatic and highly conjugated substances is well known[67,68] and shows

313   increasing efficiency at higher wavelengths, as it is observed here; on the other hand, aggregation of HS

314   by cation binding is well known.[69] Starting from this assumption, the quenching can be rationalized in

315   the following way, considering the process schematically depicted in Figure 8. When Pb(II) is added, it

316   first binds in bidentate form promoting aggregation by bridging two humic molecules; one or several

317   metal ions are expected to participate in the bridging. This process corresponds to the high affinity part

318   of the spectrum, which is thus assumed to correspond to bidentate complexation, but not necessarily all

319   Pb(II) bound in this way participate in bridging. Further increase in Pb(II) concentration results in singly

320   coordinated binding to carboxylate groups, corresponding to the low affinity part.

321   The process for the high affinity sites, which causes quenching, can be written as

322 $$2HA + nPb^{2+} \rightleftharpoons (HA)_2Pb_n$$ (11)

323   where n is the average number of Pb^{2+} ions bridging humic molecules, considering the HA

324   heterogeneity. The reaction will have a conditional equilibrium constant given by

325 $$K = \frac{[(HA)_2Pb_n]}{[HA]^2 c_{Pb}^n}$$ (12)

326   where c_{Pb} is the free Pb(II) concentration. Now, if it is assumed that free HA molecules show emission

327   whereas those bound do not, it can be written for the total fluorophore concentration F_0:[51]

328 $$F_0 = F + 2C$$ (13)

329   where F is the concentration of free fluorophores and C is the complexed fluorophores (not emitting)

330   concentration. Identifying F with [HA] and C with [HA$_2$Pb$_n$], it can be found from eqs 12 and 13, and

331   taking into account that fluorescent intensity is proportional to fluorophore concentration, that

332 $$\frac{I_F^0}{I_F} = \frac{F_0}{F} = \frac{1 + \sqrt{1 + 8KF_0 c_{Pb}^n}}{2}$$ (14)

333   Figure 9 shows the fit of FHA fluorophore scores (in Stern-Volmer form) to eq 14 using a common n

334   value for all curves, and different values for the product KF_0. The free Pb(II) concentration are obtained

335   from the potentiometric results with the Davies equation for activity coefficients. A good fitting is found

336   in general, the C component in some cases show a less satisfactory fitting, but it can be due to its lower

337   intensity, resulting in higher errors. EHA data shows similar fitting (Figure S11, Supporting

338   Information). All FHA curves are fit with $n = 1.6$, whereas EHA fits with $n = 1.3$. Unfortunately, K and

339   F_0 cannot be separated, because the many unknown factors; the resulting values for their product are

340   presented in Table S3, Supporting Information.

341   Thus, we conclude that fluorescence quenching is consistent with metal-induced aggregation of HS;

342   this aggregation proceeds at a molecular scale, to be distinguished of precipitation, however, more

343   experimental information is needed to confirm this mechanism. Other spectroscopic studies are

344   consistent with the present findings. Xia et al.[70] studied by X-ray absorption the interaction of Pb(II)

345   with a humic extract from a silt loam soil suggesting the presence of two C atoms in the second

346 coordination shell, which would indicate bidentate binding. A study by EPR measurements combined

347 with DFT analysis is consistent with a structure of Pb (II) bound to two carboxylates.[71]

348   Concluding, the NICA-EPN model here introduced describes adequately the binding of proton and

349 Pb(II) to humic acids; fluorescence quenching has a different dependence with Pb concentration

350 compared with potentiometric titrations: it is proposed that the addition of Pb(II) causes dimerization (or

351 aggregation) of humic molecules. Thus, fluorescent quenching senses multiligand Pb(II) binding (which,

352 from IR results, should be a chelate type complex), and the second site type (with lower affinity)

353 observed in potentiometric measurements is proposed be due to 1:1 binding.

359   **Supporting Information Available.** Additional figures and tables. Appendix A details the

360 experimental procedures, and Appendix B does the same for data analysis. This material is available free

361 of charge via the Internet at http://pubs.acs.org.

362

363   **FIGURE CAPTIONS**

364   Figure 1. Pb(II) binding curves at different pH and ionic strengths for Elliot soil humic acid (a) and

365   purified Fluka humic acid (b). The dotted lines are the NICA-Donnan predicted curves with the generic

366   recommended parameters of Milne et al.[3] 1 g L^{-1} HA in $NaClO_4$ at the ionic strengths shown.

367

368   Figure 2. Speciation of Pb(II) binding at pH = 5.5 and $I = 0.1$ M in $NaClO_4$ (1 g L^{-1} HA) for Elliot soil

369   humic acid (a) and purified Fluka humic acid (b). The closed symbols (total and high affinity binding)

370   correspond to the left side scale, and open symbols (low affinity and electrostatic binding) to the right

371   side scale.

372

373   Figure 3. Amount of metal bound (closed symbols) and relative fluorescence quenching (open symbols)

374   for simultaneous potentiometric and fluorescence titration of EHA (a) and FHA (b) with Pb(II). 20 mg

375   L^{-1} HA in $NaClO_4$ at the ionic strengths shown.

376

377   Figure 4. Fluorescence components as obtained from PARAFAC. (Top) Elliot soil humic acid, pH =

378   4.0; $I = 0.02$ M; (bottom) Purified Fluka humic acid, pH = 5.5, $I = 0.1$ M. Blue is zero intensity, red is

379   maximum (arbitrary scale). 20 mg L^{-1} HA in $NaClO_4$.

380

381   Figure 5. Scores of the fluorescence components (shown in Figure 3) deduced form PARAFAC as a

382   function of total Pb(II) concentration, for 20 mg L^{-1} FHA at pH = 5.5, $I = 0.02$ M ($NaClO_4$).

383

384   Figure 6. ATR-IR spectra of Elliot soil HA (0.28 g L^{-1}) in the absence and in the presence of Pb(II) at

385   different concentrations. pH = 5.5, $I = 0.1$ M ($NaClO_4$). See text for details.

386

387   Figure 7. Affinity spectrum found for EHA by NICA fitting (solid lines) and conditional spectra found

388   from analysis based on eq 8 of fluorometric quenching experiments (dashed lines).

389

390   Figure 8. Simplified scheme of the humic-Pb(II) interaction. In the first stage (high affinity sites) the

391   Pb^{2+} ions promote aggregation of humic molecules through bridging; the Pb ions bind to carboxylate

392   groups in chelate form as indicated by IR results. In the second stage, 1:1 binding takes place yielding

393   the low affinity sites; mainly single bond Pb binding is assumed, as suggested by IR results.

394

395   Figure 9. Stern-Volmer plots as a function of free Pb(II) concentrations for FHA fluorophores (symbols).

396   Lines show the fitting to eq 14.

397

398

399

400

401

402

403

404

405　　REFERENCES

406　　(1)　Senesi, N.; Loffredo, E. The Chemistry of Soil Organic Matter. In *Soil Physical Chemistry*;

407　　Sparks, D. L., Ed.; CRC Press: Boca Raton, Fl, 1998; pp. 239–370.

408　　(2)　Baldock, J. A.; Nelson, P. N. Soil Organic Matter. In *Handbook of Soil Science*; M. L. Sumner,

409　　ed.; CRC: Boca Raton, Fl, 1999; pp. B75–B84.

410　　(3)　Milne, C. J.; Kinniburgh, D. G.; van Riemsdijk, W. H.; Tipping, E. Generic NICA−Donnan

411　　Model Parameters for Metal-Ion Binding by Humic Substances. *Environ. Sci. Technol.* **2003**, *37*, 958–

412　　971.

413　　(4)　Senesi, N. Molecular and quantitative aspects of the chemistry of fulvic acid and its interactions

414　　with metal ions and organic chemicals: Part II. The fluorescence spectroscopy approach. *Anal. Chim.*

415　　*Acta* **1990**, *232*, 77–106.

416　　(5)　Cabaniss, S. E. Forward Modeling of Metal Complexation by NOM: I. A priori Prediction of

417　　Conditional Constants and Speciation. *Environ. Sci. Technol.* **2009**, *43*, 2838–2844.

418　　(6)　Tipping, E. Humic ion-binding model VI: An improved description of the interactions of protons

419　　and metal ions with humic substances. *Aquat. Geochem.* **1998**, *4*, 3–48.

420　　(7)　Kinniburgh, D. G.; Van Riemsdijk, W. H.; Koopal, L. K.; Borkovec, M.; Benedetti, M. F.;

421　　Avena, M. J. Ion binding to natural organic matter: Competition, heterogeneity, stoichiometry and

422　　thermodynamic consistency. *Colloid Surface A* **1999**, *151*, 147–166.

423　　(8)　Gustafsson, J. P. Modeling the acid-base properties and metal complexation of humic substances

424　　with the Stockholm Humic Model. *J. Colloid Interf. Sci.* **2001**, *244*, 102–112.

425　　(9)　Orsetti, S.; Andrade, E. M.; Molina, F. V. Modeling ion binding to humic substances: Elastic

426　　polyelectrolyte network model. *Langmuir* **2010**, *26*, 3134–3144.

427   (10) Benedetti, M. F.; Milne, C. J.; Kinniburgh, D. G.; Van Riemsdijk, W. H.; Koopal, L. K. Metal

428   Ion Binding to Humic Substances: Application of the Non-Ideal Competitive Adsorption Model.

429   *Environ. Sci. Technol.* **1995**, *29*, 446–457.

430   (11) Smith, D. S.; Kramer, J. R. Multisite metal binding to fulvic acid determined using

431   multiresponse fluorescence. *Anal. Chim. Acta* **2000**, *416*, 211–220.

432   (12) Bro, R. Exploratory study of sugar production using fluorescence spectroscopy and multi-way

433   analysis. *Chemom. Intell. Lab. Syst.* **1999**, *46*, 133–147.

434   (13) Stedmon, C. A.; Bro, R. Characterizing dissolved organic matter fluorescence with parallel

435   factor analysis: A tutorial. *Limnol. Oceanogr.: Methods* **2008**, *6*, 572–579.

436   (14) Ohno, T.; Amirbahman, A.; Bro, R. Parallel Factor Analysis of Excitation–Emission Matrix

437   Fluorescence Spectra of Water Soluble Soil Organic Matter as Basis for the Determination of

438   Conditional Metal Binding Parameters. *Environ. Sci. Technol.* **2008**, *42*, 186–192.

439   (15) Santín, C.; Yamashita, Y.; Otero, X.; Álvarez, M.; Jaffé, R. Characterizing humic substances

440   from estuarine soils and sediments by excitation-emission matrix spectroscopy and parallel factor

441   analysis. *Biogeochemistry* **2009**, *96*, 131–147.

442   (16) Ishii, S. K. L.; Boyer, T. H. Behavior of Reoccurring PARAFAC Components in Fluorescent

443   Dissolved Organic Matter in Natural and Engineered Systems: A Critical Review. *Environ. Sci. Technol.*

444   **2012**, *46*, 2006–2017.

445   (17) Patel-Sorrentino, N.; Mounier, S.; Benaim, J. Y. Excitation-emission fluorescence matrix to

446   study pH influence on organic matter fluorescence in the Amazon basin rivers. *Water Res.* **2002**, *36*,

447   2571–2581.

448   (18) Stedmon, C. A.; Markager, S.; Bro, R. Tracing dissolved organic matter in aquatic environments

449   using a new approach to fluorescence spectroscopy. *Mar. Chem.* **2003**, *82*, 239–254.

450   (19) Milne, C. J.; Kinniburgh, D. G.; Tipping, E. Generic NICA-Donnan Model Parameters for

451   Proton Binding by Humic Substances. *Environ. Sci. Technol.* **2001**, *35*, 2049–2059.

452   (20) Clapp, C. E.; Hayes, M. H. B.; Simpson, A. J.; Kingery, W. L. Chemistry of soil organic matter.

453   In *Chemical Processes in Soils*; Tabatabai, M. A.; Sparks, D. L., Eds.; Soil Science Society of America:

454   Madison, Wisconsin, 2005; pp. 1–150.

455   (21) Duval, J. F. L.; Wilkinson, K. J.; Van Leeuwen, H. P.; Buffle, J. Humic Substances Are Soft and

456   Permeable: Evidence from Their Electrophoretic Mobilities. *Environ. Sci. Technol.* **2005**, *39*, 6435–

457   6445.

458   (22) Dinar, E.; Mentel, T. F.; Rudich, Y. The density of humic acids and humic like substances

459   (HULIS) from fresh and aged wood burning and pollution aerosol particles. *Atmos. Chem. Phys.* **2006**,

460   *6*, 5213–5224.

461   (23) Flory, P. J. Statistical Mechanics of Swelling of Network Structures. *J. Chem. Phys.* **1950**, *18*,

462   108–111.

463   (24) Orsetti, S.; Andrade, E. M.; Molina, F. V. Application of a constrained regularization method to

464   extraction of affinity distributions: Proton and metal binding to humic substances. *J. Colloid Interf. Sci.*

465   **2009**, *336*, 377–387.

466   (25) Milne, C. J.; Kinniburgh, D. G.; De Wit, J. C. M.; Van Riemsdijk, W. H.; Koopal, L. K.

467   Analysis of proton binding by a peat humic acid using a simple electrostatic model. *Geochim.*

468   *Cosmochim. Acta* **1995**, *59*, 1101–1112.

469   (26) Christl, I.; Metzger, A.; Heidmann, I.; Kretzschmar, R. Effect of Humic and Fulvic Acid

470   Concentrations and Ionic Strength on Copper and Lead Binding. *Environ. Sci. Technol.* **2005**, *39*, 5319–

471   5326.

472   (27) Tejedor-Tejedor, M. I.; Anderson, M. A. "In situ" ATR-Fourier transform infrared studies of the

473   goethite (α-FeOOH)-aqueous solution interface. *Langmuir* **1986**, *2*, 203–210.

474   (28) Orsetti, S.; Quiroga, M. M.; Andrade, E. M. Binding of Pb(II) in the system humic acid/goethite

475   at acidic pH. *Chemosphere* **2006**, *65*, 2313–2321.

476   (29) Lourakis,   M.   Levenberg-Marquardt   in   C/C++   http://www.ics.forth.gr/~lourakis/levmar/

477   (accessed Feb 24, 2013).

478   (30) Matynia, A.; Lenoir, T.; Causse, B.; Spadini, L.; Jacquet, T.; Manceau, A. Semi-empirical proton

479   binding constants for natural organic matter. *Geochimica et Cosmochimica Acta* **2010**, *74*, 1836–1851.

480   (31) Deshmukh, A. P.; Pacheco, C.; Hay, M. B.; Myneni, S. C. B. Structural environments of

481   carboxyl groups in natural organic molecules from terrestrial systems. Part 2: 2D NMR spectroscopy.

482   *Geochimica et Cosmochimica Acta* **2007**, *71*, 3533–3544.

483   (32) Kirishima, A.; Ohnishi, T.; Sato, N.; Tochiyama, O. Determination of the phenolic-group

484   capacities of humic substances by non-aqueous titration technique. *Talanta* **2009**, *79*, 446–453.

485   (33) Mcknight, D. M.; Wershaw, R. L. Complexation of Copper by Fulvic Acid from the Suwannee

486   River- Effect of Counter-Ion Concentration. In *Humic Substances in the Suwannee River, Georgia:*

487   *Interactions, Properties, and Proposed Structures*; Averett, R. C.; Leenheer, J. A.; McKnight, D. M.;

488   Thorn, K. A., Eds.; U.S. Geological Survey, 1989; pp. 59–79.

489   (34) Czerwinski, K. R.; Kim, J. I.; Rhee, D. S.; Buckau, G. Complexation of trivalent actinide ions

490   (Am3+, Cm3+) with humic acid: The effect of ionic strength. *Radiochimica Acta* **1996**, *72*, 179–187.

491   (35) Robertson, A. P. Ph. D. Dissertation, Stanford University, CA, 1996.

492   (36) Chakraborty, P.; Chakrabarti, C. L. Competition from Cu(II), Zn(II) and Cd(II) in Pb(II) binding

493   to Suwannee River Fulvic Acid. *Water, Air, and Soil Pollution* **2008**, *195*, 63–71.

494   (37) Puy, J.; Galceran, J.; Huidobro, C.; Companys, E.; Samper, N.; Garcés, J. L.; Mas, F.

495   Conditional affinity spectra of Pb2+-humic acid complexation from data obtained with AGNES.

496   *Environmental Science and Technology* **2008**, *42*, 9289–9295.

497   (38) Quan, G.; Yan, J. Binding constants of lead by humic and fulvic acids studied by anodic

498   stripping square wave voltammetry. *Russian Journal of Electrochemistry* **2010**, *46*, 90–94.

499   (39) David, C.; Mongin, S.; Rey-Castro, C.; Galceran, J.; Companys, E.; Garcés, J. L.; Salvador, J.;

500   Puy, J.; Cecilia, J.; Lodeiro, P.; Mas, F. Competition effects in cation binding to humic acid: Conditional

501   affinity spectra for fixed total metal concentration conditions. *Geochimica et Cosmochimica Acta* **2010**,

502   *74*, 5216–5227.

503   (40) Gustafsson, J. P.; Tiberg, C.; Edkymish, A.; Kleja, D. B. Modelling lead(II) sorption to

504   ferrihydrite and soil organic matter. *Environ. Chem.* **2011**, *8*, 485–492.

505   (41) Ahmetli, G.; Yel, E.; Deveci, H.; Bravo, Y.; Bravo, Z. Investigation of Pb(II) adsorption onto

506   natural and synthetic polymers. *Journal of Applied Polymer Science* **2012**, *125*, 716–724.

507   (42) Lin, D.; Tian, X.; Li, T.; Zhang, Z.; He, X.; Xing, B. Surface-bound humic acid increased Pb2+

508   sorption on carbon nanotubes. *Environmental Pollution* **2012**, *167*, 138–147.

509   (43) Saar, R. A.; Weber, J. H. Comparison of spectrofluorometry and ion-selective electrode

510   potentiometry for determination of complexes between fulvic acid and heavy-metal ions. *Anal. Chem.*

511   **1980**, *52*, 2095–2100.

512   (44) Liu, A.; Gonzalez, R. D. Modeling adsorption of copper(II), cadmium(II) and lead(II) on purified

513   humic acid. *Langmuir* **2000**, *16*, 3902–3909.

514   (45) Fasfous, I. I.; Chakrabarti, C. L.; Murimboh, J.; Yapici, T. Complexation of lead in model

515   solutions of humic acid: Heterogeneity and effects of competition with copper, nickel, and zinc.

516   *Environ. Chem.* **2006**, *3*, 276–285.

517   (46) Ryan, D. K.; Weber, J. H. Fluorescence quenching titration for determination of complexing

518   capacities and stability constants of fulvic acid. *Anal. Chem.* **1982**, *54*, 986–990.

519   (47) Yamashita, Y.; Jaffé, R. Characterizing the Interactions between Trace Metals and Dissolved

520   Organic Matter Using Excitation−Emission Matrix and Parallel Factor Analysis. *Environmental Science*

521   *& Technology* **2008**, *42*, 7374–7379.

522   (48) He, Z.; Ohno, T.; Cade-Menun, B. J.; Erich, M. S.; Honeycutt, C. W. Spectral and Chemical

523   Characterization of Phosphates Associated with Humic Substances. *Soil Sci. Soc. Am. J.* **2006**, *70*, 1741.

524   (49) Hemmingsen, S. L.; McGown, L. B. Phase-resolved fluorescence spectral and lifetime

525   characterization of commercial humic substances. *Appl. Spectrosc.* **1997**, *51*, 921–929.

526   (50) Kowalczuk, P.; Cooper, W. J.; Durako, M. J.; Kahn, A. E.; Gonsior, M.; Young, H.

527   Characterization of dissolved organic matter fluorescence in the South Atlantic Bight with use of

528   PARAFAC model: Relationships between fluorescence and its components, absorption coefficients and

529   organic carbon concentrations. *Mar. Chem.* **2010**, *118*, 22–36.

530   (51) Lakowicz, J. R. *Principles of Fluorescence Spectroscopy*; 3rd ed.; Springer: New York, 2006.

531   (52) Park, J.-H. Spectroscopic characterization of dissolved organic matter and its interactions with

532   metals in surface waters using size exclusion chromatography. *Chemosphere* **2009**, *77*, 485–494.

533   (53) Chen, W.; Westerhoff, P.; Leenheer, J. A.; Booksh, K. Fluorescence Excitation−Emission

534   Matrix Regional Integration to Quantify Spectra for Dissolved Organic Matter. *Environ. Sci. Technol.*

535   **2003**, *37*, 5701–5710.

536   (54) Leenheer, J. A.; Croué, J.-P. Peer Reviewed: Characterizing Aquatic Dissolved Organic Matter.

537   *Environ. Sci. Technol.* **2003**, *37*, 18A–26A.

538   (55) Cory, R. M.; McKnight, D. M. Fluorescence Spectroscopy Reveals Ubiquitous Presence of

539   Oxidized and Reduced Quinones in Dissolved Organic Matter. *Environ. Sci. Technol.* **2005**, *39*, 8142–

540   8149.

541   (56) Miller, M.; Simone, B.; McKnight, D.; Cory, R.; Williams, M.; Boyer, E. New light on a dark

542   subject: comment. *Aquatic Sciences - Research Across Boundaries* **2010**, *72*, 269–275.

543   (57) Hay, M. B.; Myneni, S. C. B. Structural environments of carboxyl groups in natural organic

544   molecules from terrestrial systems. Part 1: Infrared spectroscopy. *Geochim. Cosmochim. Acta* **2007**, *71*,

545   3518–3532.

546   (58) Nakamoto, K. *Infrared and Raman Spectra of Inorganic and Coordination Compounds,*

547   *Applications in Coordination, Organometallic, and Bioinorganic Chemistry*; Part B.; John Wiley &

548   Sons: Hoboken, NJ, 2009.

549   (59) Zhang, J.; Dai, J.; Wang, R.; Li, F.; Wang, W. Adsorption and desorption of divalent mercury

550   (Hg2+) on humic acids and fulvic acids extracted from typical soils in China. *Colloids and Surfaces A:*

551   *Physicochemical and Engineering Aspects* **2009**, *335*, 194–201.

552   (60) Coates, J. Interpretation of Infrared Spectra. A Practical Approach. In *Encyclopedia of Analyical*

553   *Chemistry*; Meyers, R. A., Ed.; John Wiley & Sons: Chichester, UK, 2000; pp. 10815–10837.

554   (61) Cabaniss, S. E.; Shuman, M. S. Combined ion selective electrode and fluorescence quenching

555   detection for copper-dissolved organic matter titrations. *Anal. Chem.* **1986**, *58*, 398–401.

556   (62) Marang, L.; Reiller, P. E.; Eidner, S.; Kumke, M. U.; Benedetti, M. F. Combining Spectroscopic

557   and Potentiometric Approaches to Characterize Competitive Binding to Humic Substances.

558   *Environmental Science & Technology* **2008**, *42*, 5094–5098.

559   (63) Alcock, N. W.; Tracy, V. M.; Waddington, T. C. Acetates and acetato-complexes. Part 2.

560   Spectroscopic studies. *J. Chem. Soc., Dalton Trans.* **1976**, 2243–2246.

561   (64) Cabaniss, S. E. Quantitative Structure−Property Relationships for Predicting Metal Binding by

562   Organic Ligands. *Environ. Sci. Technol.* **2008**, *42*, 5210–5216.

563   (65) Steiner, R. F.; Kirby, E. P. Interaction of the ground and excited states of indole derivatives with

564   electron scavengers. *J. Phys. Chem.* **1969**, *73*, 4130–4135.

565   (66) Kumke, M. U.; Eidner, S. Fluorescence and Energy Transfer Processes of Humic Substances and

566   Related Model Compounds in Terbium Complexes. In *Humic Substances: Molecular Details and*

567   *Applications in Land and Water Conservation*; Ghabbour, E. A.; Davies, G., Eds.; Taylor & Francis,

568   2005; pp. 131–152.

569   (67) Lavorel, J. Influence of Concentration on the Absorption Spectrum and the Action Spectrum of

570   Fluorescence of Dye Solutions. *J. Phys. Chem.* **1957**, *61*, 1600–1605.

571   (68) West, W.; Pearce, S. The Dimeric State of Cyanine Dyes. *J. Phys. Chem.* **1965**, *69*, 1894–1903.

572   (69) Senesi, N.; Loffredo, E. Metal Ion Complexation by Soil Humic Substances. In *Chemical*

573   *Processes in Soils*; Tabatabai, M. A.; Sparks, D. L., Eds.; SSSA Book Series; Soil Science Society of

574   America: Madison, Wisconsin, 2005; pp. 563–617.

575   (70) Xia, K.; Bleam, W.; Helmke, P. A. Studies of the nature of Cu2+ and Pb2+ binding sites in soil

576   humic substances using X-ray absorption spectroscopy. *Geochim. Cosmochim. Acta* **1997**, *61*, 2211–

577   2221.

578   (71) Witwicki, M.; Jerzykiewicz, M.; Jaszewski, A. R.; Jezierska, J.; Ozarowski, A. Influence of

579   Pb(II) Ions on the EPR Properties of the Semiquinone Radicals of Humic Acids and Model Compounds:

580   High Field EPR and Relativistic DFT Studies. *J. Phys. Chem. A* **2009**, *113*, 14115–14122.
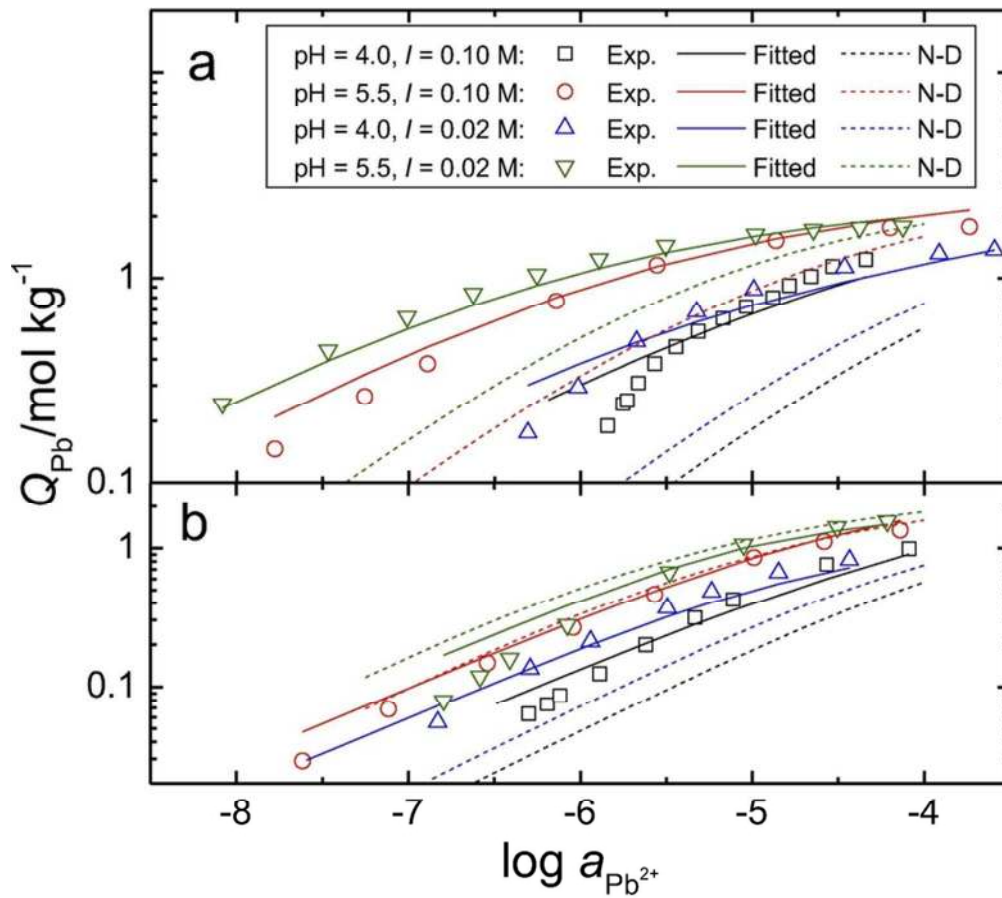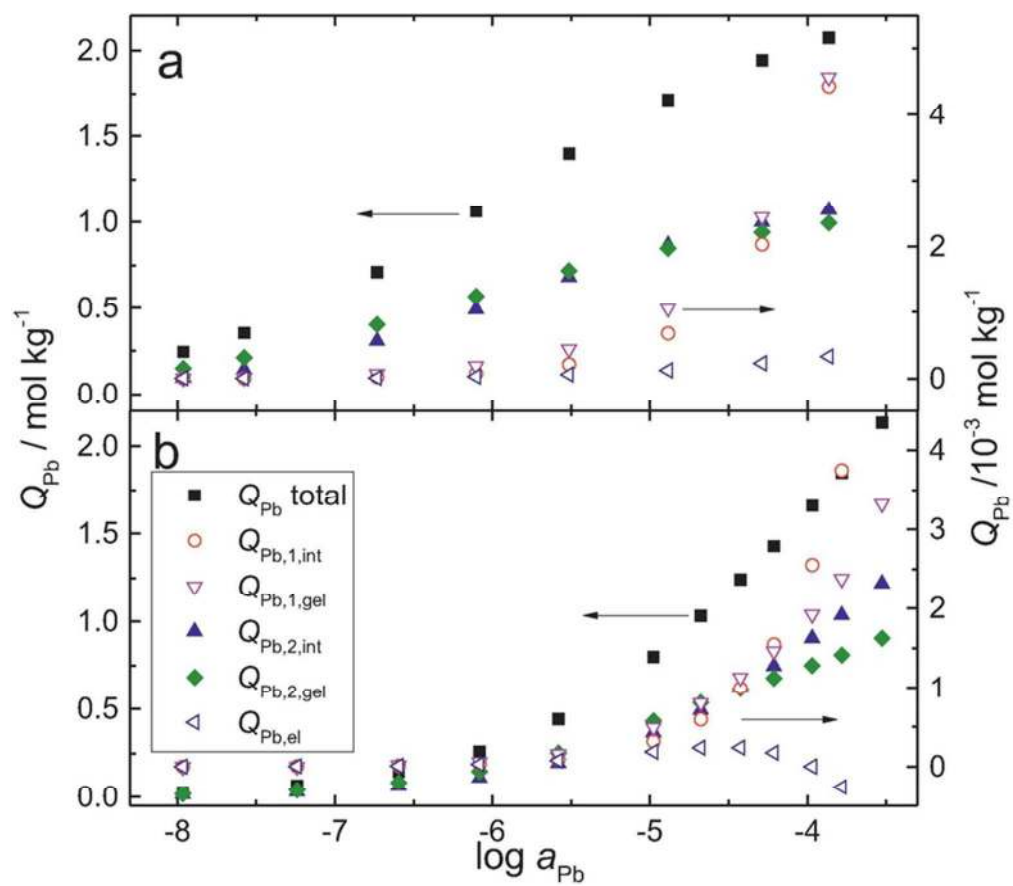
581

582

Figure 1
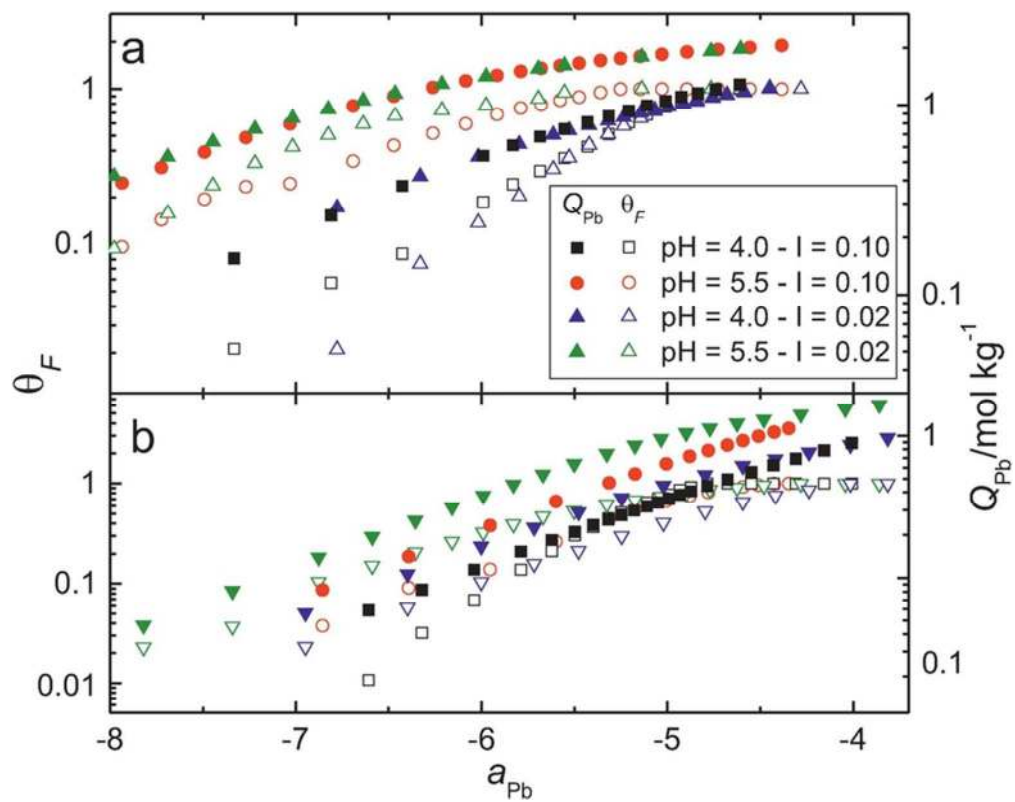71x63mm (300 x 300 DPI)

Figure 2
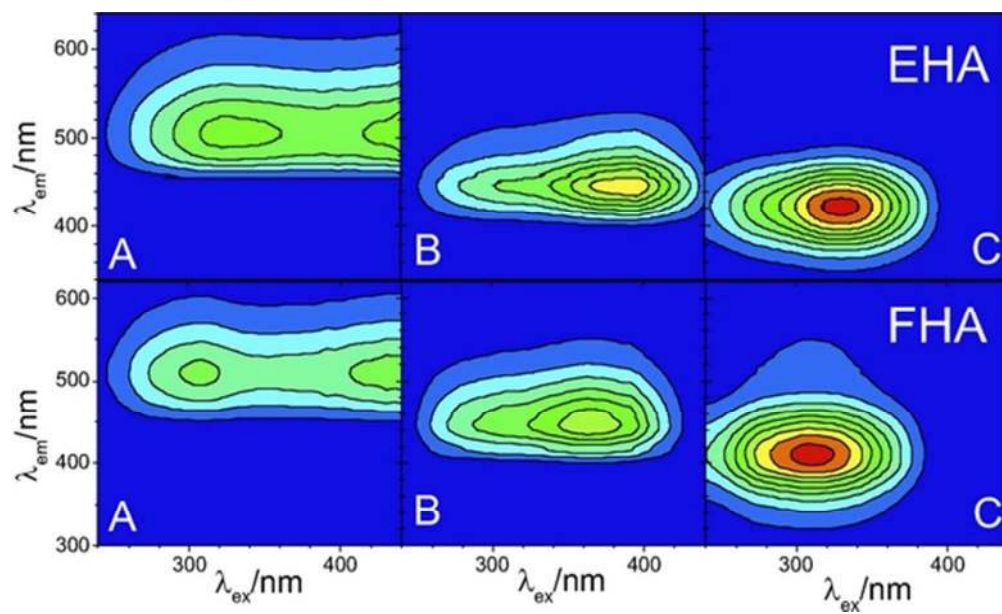70x61mm (300 x 300 DPI)

Figure 3
72x57mm (300 x 300 DPI)

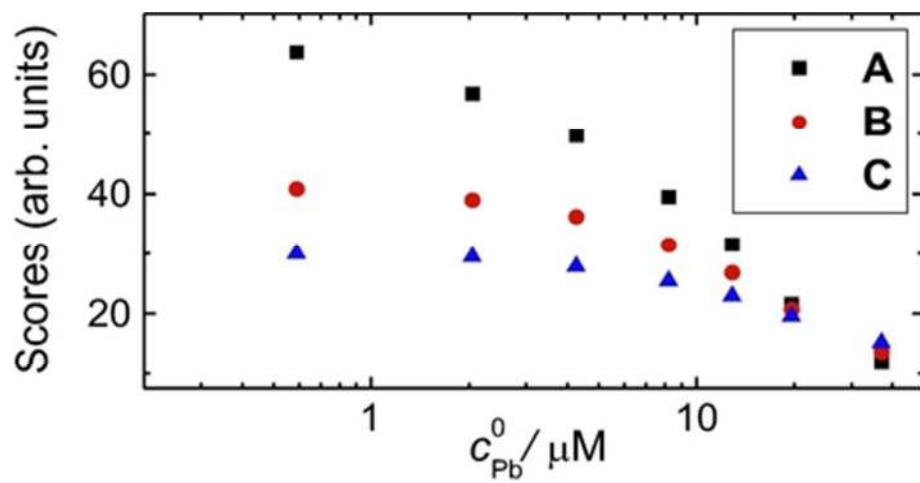Figure 4
50x30mm (300 x 300 DPI)
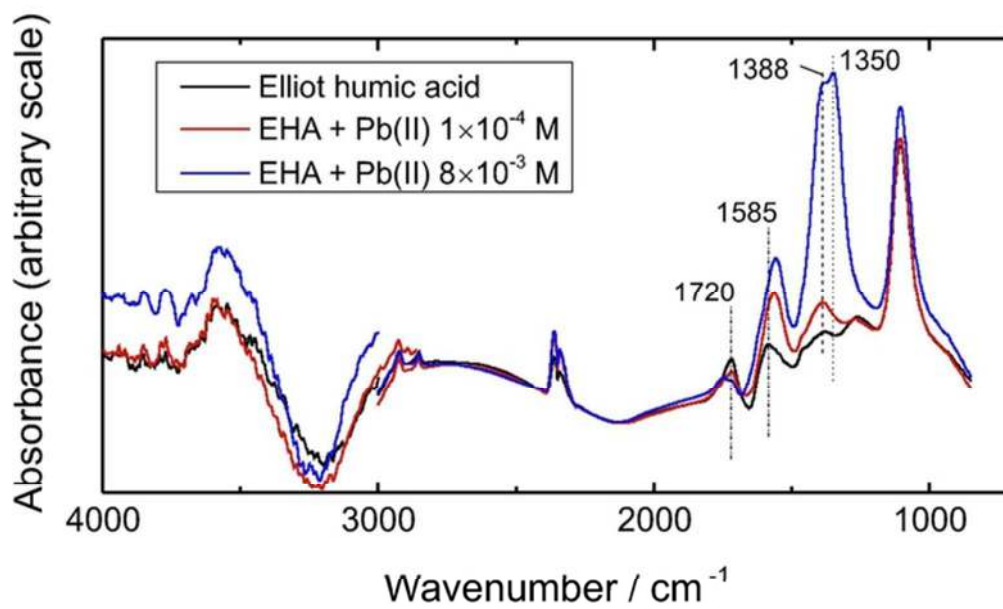
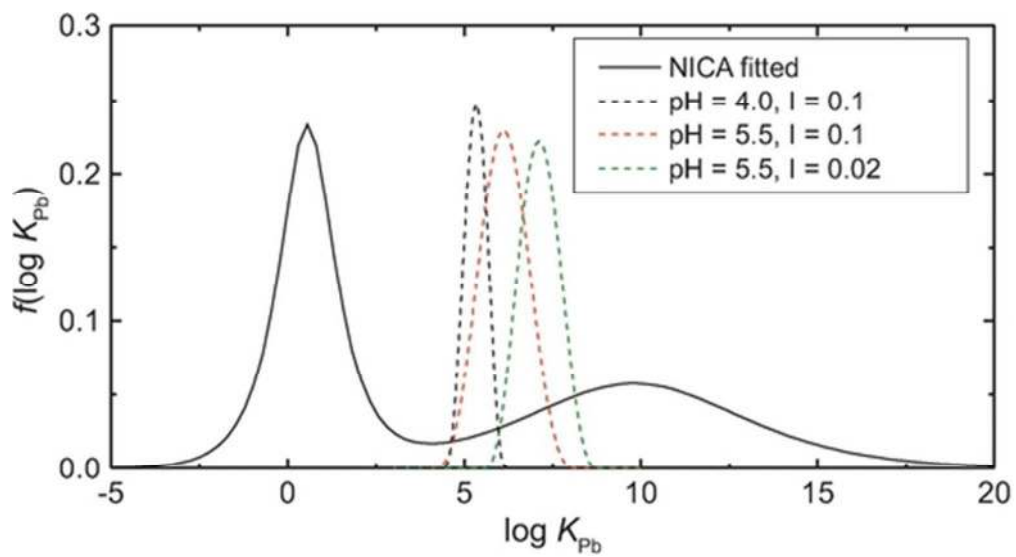Figure 5
38x19mm (300 x 300 DPI)

Figure 6
58x39mm (300 x 300 DPI)
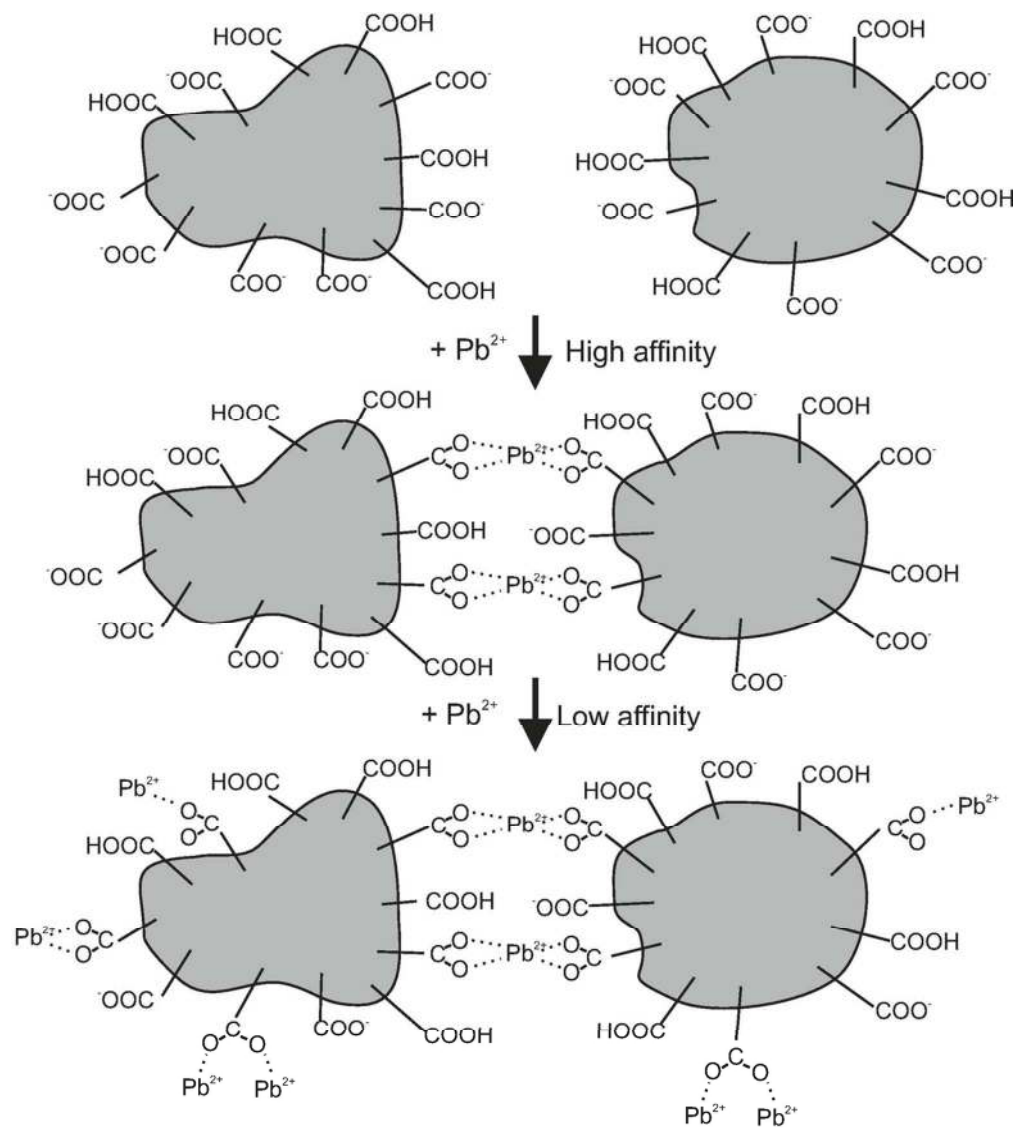
Figure 7
46x25mm (300 x 300 DPI)
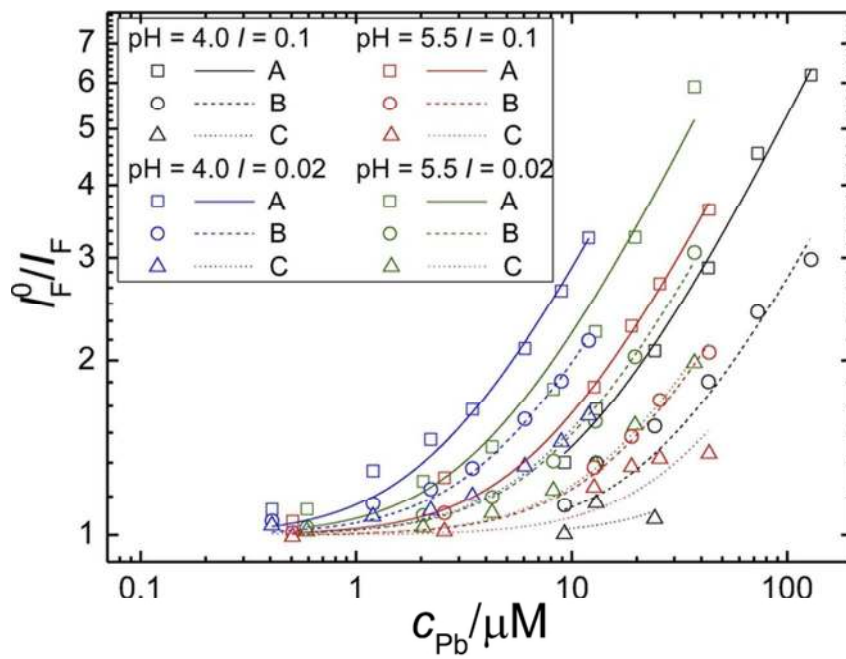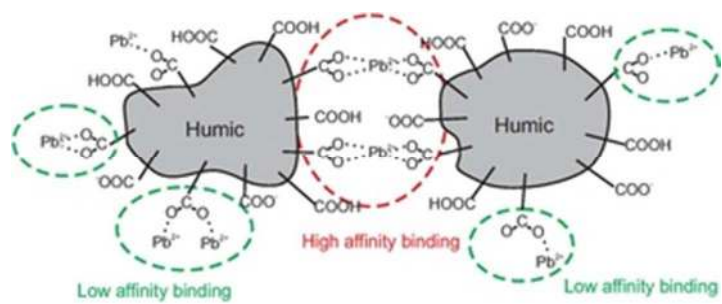
Figure 8
101x113mm (300 x 300 DPI)

Figure 9
75x51mm (300 x 300 DPI)

TOC Art
29x12mm (300 x 300 DPI)